Engineering Journal issn: 0125-8281

Article

Numerical Simulation of Currents and Volume Transport in the Malacca Strait and Part of South China Sea

Yudi Haditiar[1,a], Mutiara R. Putri[2], Nazli Ismail[3], Zainal A. Muchlisin[1,4], and Syamsul Rizal[1,5,b,*]

1 Graduate School of Mathematics and Applied Sciences, Universitas Syiah Kuala, Banda Aceh 23111, Indonesia
2 Department of Oceanography, Bandung Institute of Technology, Bandung 40132, Indonesia
3 Department of Physics, Universitas Syiah Kuala, Banda Aceh 23111, Indonesia
4 Department of Aquaculture, Faculty of Marine and Fisheries, Universitas Syiah Kuala, Banda Aceh 23111, Indonesia
5 Department of Marine Sciences, Faculty of Marine and Fisheries, Universitas Syiah Kuala, Banda Aceh, 23111, Indonesia
E-mail: [a]yudi.h@mhs.unsyiah.ac.id, [b]syamsul.rizal@unsyiah.net (Corresponding author)

Abstract. This work aimed to determine the hydrodynamics of the Malacca Strait (MS) and the part of the South China Sea (SCS). The study uses the two-dimensional numerical model with a finite-difference method. The results show that the sea surface heights in MS and the part of SCS are reversed and consistent with assimilation data that derived from Simple Ocean Data Assimilation (SODA). Sea surface in northern MS is lower than that in the southern part during January and July. However, the interval of SSH in both January and July appears differently. It is steeper in January than in July. Therefore, the currents and transports during January are stronger than those during July. However, the direction of currents and volume transport of MS flow to the Andaman Sea both in January and July. In part of SCS, the pattern is relatively the same as in MS; that is, the currents during January are stronger than those during July. In general, mostly volume transport in MS is going to the Andaman Sea and volume transport from part of SCS is deflected to the southern part of MS, especially in January.

Keywords: Monsoons, sea surface height, currents, Malacca Strait, South China Sea.

ENGINEERING JOURNAL Volume 23 Issue 6
Received 18 April 2019
Accepted 24 October 2019
Published 30 November 2019
Online at http://www.engj.org/
DOI:10.4186/ej.2019.23.6.129

DOI:10.4186/ej.2019.23.6.129

1. Introduction

The Malacca Strait (MS) has a vital role in the Asian economy, especially for Singapore, Malaysia, and Indonesia, because it connects the world oil trader and world shipping lane. MS also has fisheries resources [1] and marine renewable energy that valuable for around countries [2] and energy security [3]. That condition makes high sea traffic activities, marine accidents, and environmental pollution in MS. Therefore, the hydrometeorology information as the movement of wind and current is required [4].

The magnitude of wind in MS tends to vary spatially, and its effect on currents might not periodic compared to tides. Chen et al. [5] reported that wind has a great effect on northern MS. It can even disrupt the effect of the tides. The wind can modify sea surface that can drive a complex current circulation. According to Siripong et al. [4], the current can cause the transport of contaminated water.

Numerical study in MS has been carried out by several authors. Rizal and Sündermann [6] simulated MS and calculated its transport and energy due to tides. Haditiar et al. [7] have compared the effect of bottom friction on hydrodynamics in MS during February and August. They found that the bottom friction variables greatly affect the ocean currents in MS. Chen et al. [5] also have analyzed the ocean current in MS using wind and tide effects. They showed the importance of wind on the MS circulation. Subramanian [8] by using the hydrostatic approximation and dispersion model, concluded that seasonal monsoon reversal contributes to the pollutant transport in MS.

In general, ocean current in MS, both in February (NE monsoon) and in August (SW monsoon), comes from the south of MS to the Andaman Sea [9, 10]. The current direction in MS is due to the difference in the sea surface. According to Wyrtki [11], most of the year, the sea surface height in southern MS is higher than in northern MS. Furthermore, Tay et al. [12] concluded that an anomaly of the sea surface in MS is determined by the monsoon.

Even though the current flows from south to north of MS, both in January (NE monsoon) and in August (SW monsoon), their transport does not have to be the same [8]. In addition, they can also be affected by the adjacent sea. The Indian Ocean and the part of South China Sea (SCS) are connected by MS via the Karimata Strait so that the hydrodynamic changes in part of SCS may affect MS. The effect of monsoon not only can be seen in MS but also in the Gulf of Thailand (GoT). In central and south of GoT (around 7.17- 9.78 N), the residual surface currents change seasonally between NE and SW monsoon [13]. Meanwhile, in the north of GoT, the counter-clockwise and clockwise circulation can be seen during NE and SW monsoon, respectively [14].

The study of transport in MS has been carried out by [15-18]. They have calculated transport across several straits in SCS region such as the Taiwan Strait, Balabac, Mindoro, Luzon, Karimata, and MS. Studies have suggested that the Karimata Strait links the Java Sea and the MS to the Andaman Sea, respectively; SCS water is moved to the Sulu, Java, and Andaman Seas, via the aforementioned straits, respectively; then, in the end, it merges into the Indian Ocean. Fang et al. [15] reported that the western Pacific water goes into the SCS through the Luzon Strait with the average annual (from 1982 to 2003) volume being 4.80 Sv, where 1.71 Sv goes back to the western Pacific waters through the Taiwan Strait and the East China Sea, and 3.09 Sv enters the Indian Ocean. Moreover, the mean transport via MS (from the surface to the depth 58 m) is only 0.16 Sv. Fang et al. [15-18] showed that the transport in MS is smaller than that in the Karimata Strait and the Taiwan Strait. In the Southwest Monsoon (SW Monsoon) period, transport in MS is very small compared to the one in the Taiwan Strait that is very large. However, based on observation [11], MS facilitates a small water mass exchange between the Sunda Shelf and the Indian Ocean that important to the Pacific and Indian Ocean connection. Moreover, Daryabor et al. [19] showed that the volume transport from SCS to the Andaman Sea through MS is quite large. According to them, in January, volume transport through MS was about 1.8 Sv by using ROMS and 1.4 Sv from SODA.

Computational fluid dynamics are quite well for fluid flow, current prediction, mass transfer, and heat transfer problems [20, 21]. Kalakan et al. [22] added that computational fluid using the two-dimensional numerical model is good enough for predicting coastal flooding. In this study, we would like to calculate and verify the current and transport in MS by using the computational fluid dynamics, i.e., two-dimensional numerical model. The model is given the external forces, that is, SSH and wind forcing. Many researchers use the Sea Surface Height (SSH) and wind in transport volume studies, such as in the Western Labrador Sea [23], Malvinas, Brazil [24], Agulhas current system [25], and Singapore coastal Waters [26]. Tang and Hang [23] reported that the total volume transport in the Western Labrador Sea (6.2 Sv) has a positive correlation with the wind patterns and the fall or winter North Atlantic Oscillation (NAO) index. Also, Vivier and Provost [24] found a high relationship between the volume transport derived from SSH and the volume

transport from the current meter ($r = 0.8$) during three-year time-series observations in Malvinas. According to Vermeulen et al. [25], establishing a linear relationship between cross-current SSH gradients and volume transport measurements can improve the skill of the Agulhas transport. Xu and Chua [26] report that in the sea model simulation, the surface height is essential for the calculation of monthly volumes transport in MS and Singapore Strait.

The domain of this study includes MS and a small part of SCS (Fig. 1). MS is located between Peninsular Malaysia and Sumatra. Its length is about 980 km, varying in width from 445 km in the north to 52 km in the south [6]. In MS, the depth of MS is about 400 and 20 meters for maximum and minimum, respectively, while the mean depth is about 50 meters.

2. Material and Methods

2.1. Data Used in Numerical Setup

To simulate the current and transport in MS we need the following data:

(1) Topographic data 5' x 5' are obtained from SRTM30. SRTM30 is a near-global digital elevation model (DEM) comprising a combination of data from the Shuttle Radar Topography Mission and the U.S. Geological Survey's GTOPO30 data set. The data can be downloaded for free from ftp://topex.ucsd.edu/pub/srtm30 plus/.

(2) Data of 4-times daily wind vectors are obtained from NCEP Reanalysis I. The wind data have interpolated using HAMSOM preparing methods [27] and the original data can be accessed in [28].

(3) Open boundary models are indicated by the red square edges in Fig. 1. Open boundary values are obtained from SSH of Simple Ocean Data Assimilation (SODA) v2.2.4. [29, 30]. The resolution of data is $\Delta x=\Delta y= 0.5^\circ$ and available only monthly average. SODA is reanalysis data that has been verified using many observation data (World Ocean Atlas 1994, expandable bathythermograph, CTD, and altimetry satellite (Geosat, ERS/1, TOPEX/Poseidon)). Therefore, SODA can represent the influence of global or regional ocean circulation. The data can be accessed in https://iridl.ldeo.columbia.edu/SOURCES/.CARTON-GIESE/.SODA/.v2p2p4/.

(4) Hybrid Coordinate Ocean Model (HYCOM) is used to compare numerical current results [31].

2.2. Numerical Model Setup

In order to solve the momentum equations for *x-y* component, by using the continuity, advection, wind stress, bottom stress, and diffusion equation we use the numerical scheme and method for two-dimensional model [32]. The advection terms ($u\ du/dx + v\ du/dy$ and $u\ dv/dx + v\ dv/dy$) were solved by Total Variation Diminishing (TVD) superbee and the detail of this method can be seen in [32].

The equations used are the following.

Momentum equations:

$$\frac{\partial u}{\partial t}+u\frac{\partial u}{\partial x}+v\frac{\partial u}{\partial y}-fv=-g\frac{\partial \eta}{\partial x}+\frac{\tau_x^{wind}-\tau_x^{bot}}{\rho_0 h}+\frac{\partial}{\partial x}\left(A_H\frac{\partial u}{\partial x}\right)+\frac{\partial}{\partial y}\left(A_H\frac{\partial u}{\partial y}\right) \quad (1)$$

$$\frac{\partial v}{\partial t}+u\frac{\partial v}{\partial x}+v\frac{\partial v}{\partial y}+fu=-g\frac{\partial \eta}{\partial y}+\frac{\tau_y^{wind}-\tau_y^{bot}}{\rho_0 h}+\frac{\partial}{\partial x}\left(A_H\frac{\partial v}{\partial x}\right)+\frac{\partial}{\partial y}\left(A_H\frac{\partial v}{\partial y}\right) \quad (2)$$

where the current velocities in two dimensions are defined by $u(t,x,y)$ and $v(t,x,y)$. Meanwhile f is Coriolis parameter, $\eta(x,y,t)$ is sea level elevation or SSH, ρ_0 is sea water density, g is gravitation, and h undisturbed seawater depths.. The viscosity coefficient of horizontal is A_H.

Continuity equation:

$$\frac{\partial \eta}{\partial t} + \frac{\partial \left(h\langle u \rangle\right)}{\partial x} + \frac{\partial \left(h\langle v \rangle\right)}{\partial y} = 0\,, \tag{3}$$

where h is depth.

Wind stress equations:

$$\tau_x^{wind} = \rho_{air} C_d U_{wind} \sqrt{\left(U_{wind}\right)^2 + \left(V_{wind}\right)^2} \tag{4}$$

$$\tau_y^{wind} = \rho_{air} C_d V_{wind} \sqrt{\left(U_{wind}\right)^2 + \left(V_{wind}\right)^2} \tag{5}$$

where the wind stress is defined by $\tau^{wind}(x,y)$, ϱ_{air} is wind density, C_d is non-dimensional wind drag coefficient. U_{wind} and V_{wind} are the zonal and meridional wind velocities above 10 meters of the ocean surface, respectively. Bottom frictions on topography in x and y, respectively ($\tau^{bot}(x,y)$), are given by

$$\tau_x^{bot} = \rho_0 r_b u \sqrt{u^2 + v_u^{\,2}} \tag{6}$$

$$\tau_y^{bot} = \rho_0 r_b v \sqrt{u_v^{\,2} + v^2} \tag{7}$$

where r_b is non-dimensional bottom friction coefficient, u_v is u current velocity at v grid, v_u is v current velocity at u grid.
The volume transport can be calculated with following equation:

$$F_{vol} = \int_A v_n dA \tag{8}$$

where F_{vol} is volume transport, A is transect from surface to bottom, dA is area element, and v_n is velocity component perpendicular to transect.

We choose the domain area between 0.5°N–5.5°N and 95.5°E–105°E. The resolution in horizontal grid is $\Delta x = \Delta y = 5$' resolutions and time-step is $\Delta t = 50$ seconds (based on Courant-Friedrichs-Lewy condition). In addition, for wind coefficients are ρ_{air} = 1.184 kg m^{-3}, C_d = 1.285 (for wind < 11 m s^{-1}), r_b= 0.0025, A_H = 500 m^2 s^{-1}, and ρ_0 =1028 kg m^{-3}. The r_b and A_H coefficients are based on the previous study [9]. The coefficients are important for explaining the wind effect and bottom friction on the hydrodynamic model.

The open boundary values are given from the monthly SSH of SODA with the zero-gradient condition. Meanwhile, the wind is used as a surface boundary in the numerical simulations. We introduced the wind stress field slowly over an adjustment period of 9 days to avoid initial disturbances. The results of this numerical simulation are the monthly average of SSH, current circulation, and volume transport. The monthly SSH from the model output is verified by SODA using correlation coefficient (r) and Root Mean Square Error (RMSE) [26, 33]. Whereas the monthly circulation from the model output is validated using the monthly flow derived from HYCOM.

The equations of correlation coefficient (r) and RMSE [26, 33] as follows:

$$r = \frac{\sum \left(X_{\mathrm{mod}} - \overline{X_{\mathrm{mod}}}\right)\left(X_{obs} - \overline{X_{obs}}\right)}{\sqrt{\sum \left(X_{\mathrm{mod}} - \overline{X_{\mathrm{mod}}}\right)^2 \sum \left(X_{obs} - \overline{X_{obs}}\right)^2}} \tag{9}$$

where X_{mod} is the desired quantity to compare, that is, sea level elevation of model results. $\overline{X_{mod}}$ is the quantity averaged of X_{mod}. X_{obs} is sea level elevation of SODA. $\overline{X_{obs}}$ is the quantity averaged of X_{obs}. Meanwhile root mean square error (RMSE) is defined as follows:

$$RMSE = \sqrt{\frac{1}{n}\sum_{i=1}^{n} e_i^2} \tag{10}$$

where e_i is sea level results minus sea level SODA (i=1,2,…., n). RMSE (0 – 0.10) is a good fit, while (0.10 – 0.20) is moderate fit, and > 0.40 is poor fit [34].

3. Results and Discussions

3.1. Wind Circulation

In MS, the wind speed decreases as it approaches the Sumatra coastlines. The existence of the Sumatra Island is a barrier to wind circulation during January in MS. Meanwhile, strong wind in the northern part of MS is caused by the NE monsoon peak. NE winds in January 2010 is shown in Fig. 2 (a). The wind flows from the northeast to the southwest. In MS, the wind speed is spatially different. Strong winds are in the northern part of MS (the velocity is 1.5 m/s - 2 m/s), moderate in the middle part of MS (0.5 m/s - 1 m/s), and weak in the south part of MS (maximum speed around 0.5 m/s). During January the strongest wind speed was found in part of SCS (3 m/s - 4 m/s). The wind speed at part of SCS is seen to decrease as it approaches the Peninsular Malaysia coastline.

Figure 2(b) shows SW winds in July and the wind flows from the Indian Ocean (the south and southwest) to the north of domain. In MS, the wind velocity reaches 1 m/s, while wind velocity is about 1 m/s - 2 m/s in part of SCS. Figure 2(a) and 2(b) show SW winds in MS that are blocked by the island of Sumatra, so the magnitude of SW winds is weaker than the NE winds magnitude. However, NE wind is only dominant until the middle part of MS, while in the southern part of MS, both NE and SW winds look quite small. Based on tidal, wind, and bathymetry analysis in MS, Chen et al. [5] reported that ocean current energy due to the wind is greater in the northern part of MS than in the southern part of MS. In the northern part of MS, winds are relatively strong and can produce eddy which can disrupt current circulation.

3.2. Sea Surface Height

Figure 3 (a) and 3 (b) show the contour and interval of SSH in January 2010 and July 2010, respectively. In January, SSH is higher on the east coast of Peninsular Malaysia. It is caused by the NE winds that move water masses from part of SCS towards the coast of Peninsular Malaysia (convergent). According to Subramanian [14] during January (NE monsoon), the current from SCS is moving southward to the Java Sea. The water masses are partially deflected to MS because the sea surface in the Java Sea is higher than the Indian Ocean. Thus, this process results in a high sea surface in the southern part of MS. Wrytki [11] confirmed that SSH in the southern part of MS is relatively high throughout the year. Based on our research, SSH is higher in the south due to weak wind conditions both in January and July. Also, the effect of topography in the southern part of MS that quite narrow and shallow. The SSH and its contour (gradient of SSH) decrease from the southern part of MS to the Andaman Sea. This condition is caused by the transition of MS topographic which more narrow and shallow (less than 25 meters) in the southern part of MS compare to the northern part of MS (around 50 meters). Also, the NE wind in the northern part of MS (2 m/s) causes a low SSH in the northern part of MS. These results are following Tay et al. [12] who reported that monsoon changes produce a sea surface anomalies in MS, where the sea surfaces of the Andaman Sea are lower in January (NE monsoon) and high in July (SW monsoon), April, and October (intermonsoon). Thus, NE monsoon is essential to the distribution of SSH in the northern part of MS.

Based on Fig. 3 (b), SSH in the northern part of MS was slightly higher during July (about 0.52 meters) (Fig. 3 (b)) compared to January (about 0.46 cm) (Fig. 3 (b)). During July, the south wind and southwest wind is relatively weak in MS (Fig. 2 (b)) so that the wind has less effect on SSH in the northern part of MS. Also, southerly winds push the sea surface around the southern part of Peninsular Malaysia towards the offshores, causing SSH and SSH gradients in part of SCS are smaller in July than in January. If we compare the contours

of Fig. 3 (a) and 3 (b), it can be seen that SSH in MS is steeper in January than that in July. It is caused by is because the wind is stronger in January than in July.

To show the differences in the contribution of the monsoon to SSH spatially, we show SSH differences between January and July (sea level in January minus sea level in July) (Fig. 3 (c)). Figure 3(c) shows that the difference of SSH is greater in part of SCS compared to MS. It means that the influence of monsoon on SSH is greater in part of SCS than in MS, especially in NE monsoon. Thompson and Tkalich [35] reported that in the southern part of SCS, the highest SSH amplitude occurs around the Gulf of Thailand. This feature can be seen from NE of SCS (4°N-5°N) during January (NE monsoon) (Fig. 3(a)).

Figure 3(d) and 3(e) show SSH derived from SODA (0.5° x 0.5°) in January 2010 and July 2010, respectively. The difference is shown in Fig. 3(f). Figure 4a shows that SSH is lower in NW of MS. SSH increases from north to the south of MS. The contour of SSH is dense from 3° N to southern MS, while at part of SCS, SSH decreases as it moves away from the shoreline. Figure 4b shows the SSH in NW of MS is also lower. SSH gradually increases from north to south of MS, while, in part of SCS, the SSH is relatively the same.

We use the statistics to verify our results (Fig. 3(a) and 3(b)) and SODA (Fig. 3(d) and 3(e)). The correlation coefficients between the model results and SODA are 0.981 and 0.947, for January (Figs. 3(a) and 3(d)) and July (Fig. 3(b) and Fig. 3(e)), respectively, while both of the roots mean square error (RMSE) are 0.03 m and 0.016 m, for January and July, respectively. It means that the model results for January and July 2010 (Fig. 3(a) and 3(b)) show a good agreement with SODA for the same months (Fig. 3(d) and 3(e)). SSH in the south is always higher than in the north of MS, in both January and July. This result is consistent with our simulation.

3.3. Current Circulation

Figure 5 (a) and Figure 5 (b) show the current velocities in January and July 2010, respectively. Figure 5 (a) shows strong current in three locations, that is, north of MS, south of MS, and north of SCS (4°N-5°N). The strong current circulation in the northern part of MS is due to variations in SSH during January. SSH variations cause the current flow from Peninsular Malaysia moves into the waters of Sumatra. SSH gradient between north and south of MS causes a strong current in the south of MS. Also, the condition of the south of MS, which is relatively narrow and shallow supports the strong current. On the other hand, NE winds cause high SSH in north of SCS (4°N-5°N). The variation of SSH in part of SCS creates currents from part of SCS flow into MS and increases the current velocity in the southern part of MS. Xu and Malanotte-Rizzoli [36] have also concluded that the South China Sea Throughflow (SCSTF) follows entering the South China Sea via the Karimata Strait, a small amount of SCSTF moves northwestwards to the MS. According to Subramanian [8], the higher sea surfaces in the Java Sea causes the deflection of current circulation into the MS in January.

Figure 5 (b) shows that the current structure in MS is relatively the same as that shown in Fig. 5 (a). In the northern part of MS, although the wind speed is relatively weak, the current circulation is almost the same as the current in January (Fig. 5 (a)). It is caused by the zonal SSH gradient that is high SSH in the part of Peninsular Malaysia and low SSH in the Sumatran Waters. Meanwhile, in the southern part of MS, strong currents are caused by SSH and the influence of bottom topography. However, in July, the current velocity is weak in the southern part of MS are weaker than in January because the SSH gradient in MS is low. At part of SCS the weak currents are caused by southerly winds and small SSH gradients (SSH almost the same). However, the current at part of SCS continues to flow south towards the southern part of Peninsular Malaysia and MS.

We also show the differences in magnitude current between January and July in Fig. 5 (c). The difference in current speed is generally positive, indicating that the flow in January is greater than in July. The more current differences are observed in the southern part of MS and the northern part of SCS (4°N-5°N). These results indicate that the change of monsoon contributes significantly to variations in current speed.

Figure 5(d) and 5(e) show circulations of currents obtained from HYCOM in January and July, respectively. Figure 5(d) shows a strong current is flowing in the south of MS and part of SCS, while, in the north of MS, the currents are weak. From southern MS to middle MS, the currents flow to the northwest with high velocities. The currents look convergent at around 3° N, and then the current weakens. In part of SCS the dominant currents flow southward and parallel to the coastline. The current velocity in part of SCS is relatively the same as in southern MS. Fig. 5(e) shows the same current pattern as in Fig. 5(d). Only magnitudes in Fig. 5(e) are smaller than those of Fig. 5(d). The differences of magnitude between January

(Fig. 5(d)) and July (Fig. 5(e)) can be seen in Fig. 5(f). It shows a great difference in the south or shallow of MS.

Figure 5(a) and 5(d) show the results of current simulation and HYCOM, respectively, in January. Both figures describe the current in MS flows to the northwest, especially from the south to the middle of MS. In this section, their velocity is relatively similar. In the northern part of MS, there is a slight difference between our simulation and HYCOM currents. It is caused by the differences in the numerical model set up, where the HYCOM current used the baroclinic influences, i.e., heat flux (bulk formula), precipitation, and winds. Whereas our model only uses wind and SSH. However, in shallow regions such as the southern part of MS, the current circulation is relatively similar.

Meanwhile, in part of SCS, it can be seen that the current velocity looks slightly different. However, in general, the currents are flowing to the south. Moreover, in July the current simulation (Fig. 5(b)) and HYCOM (Fig. 5(e)) show that the current from the south until the middle of MS flows to the northwest. In Figure 5(e), the currents are smaller than those in Fig. 5(b). In southern part of SCS, both Fig. 5(b) and 5(e) show the same direction but different velocity.

3.4. Volume Transport

Figure 6(a) and 6(b) show U-transport for January and July, respectively. U-transport means transport in the east-west direction. The values are positive if the transport is to the east, and vice versa. In the north and south of MS, the transport flows to the west to the Sumatra coastline since the values are negative. The low SSH in the waters off Sumatra compares to Peninsular Malaysia resulting in negative transport. Subramanian [8] reported that during January, SCS water masses partly are deflected to the westward towards MS due to the high SSH gradient in the Java Sea.

Figure 7(a) and 7(b) show the V-transports in January and July, respectively. V-transport means transport to the north-south direction. Transport to the north is positive, while the south is negative. In the north of MS, the transport is split into two parts: one towards the Andaman Sea and another stay in MS. In the south of MS, transport flows to the north while north of SCS (4°N-5°N) transport flows to the south. The strong transport occurred in January (NE monsoon), where there is a large NE wind, current, and SSH difference between the north of MS and the south of MS. Figure 7(b) shows the transport in the north of MS still divided in two directions with the same transport direction while in southern part of MS and SCS, transport becomes smaller. In general, the SSH gradient in MS determines the power of V-transport. We also show the magnitude of the transport volume that overlaps with ocean currents in Fig.8 (a) and Fig. 8 (b). It shows that spatially, the magnitude of the transport volume at MS and part of SCS is greater in January (NE monsoon).

We calculate the transport in MS along transects of 1.5°N, 3°N and 5°N (Fig. 1) which have the values of 0.21, 0.22, and 0.21 Sv, respectively, for January. Then, we evaluate the calculation with the previous studies in MS. The location of validation is around the southern part of MS [17, 18, 19, 26]. According to GFDL MOM2 [18], GFDL MOM2 [17], ROMS [19], SODA [19], and SUNTANS [26] the volume transports in MS are 1.14, 0.43, 1.8, 1.4, and 0.0953 Sv, respectively.

For July, based on our calculation, the transports in MS along transects of 1.5^{o} N, 3^{o} N and 5^{o} N are 0.14, 0.14, and 0.13 Sv, respectively. However, the previous studies by [17, 18] found that the transports were -0.19 and -0.01 Sv, respectively. It means, according to them [17] there is a small transport flow to SCS. Differences in volume transport calculation in MS may be due to the numerical model set up, model resolution, and the open boundary condition. In our study, we include the northern of MS or Sumatran waters as the open boundary domain. All of the volume transports are summarized in Table 1.

Rizal et al. [9, 10] found that ocean current in MS, both NE monsoon and SW monsoon comes from the south of MS to the Andaman Sea, and the difference in SSH causes the currents. This dynamic produces a positive (northward) volume transport in MS. Xu and Chua [26] indicated that regular outflows the monthly mean volume transport across the MS is negative during the whole year (from MS to the Andaman Sea). The maximum and minimum westward peak values 0.0953 Sv and 0.0261 Sv had been reported in January and June, respectively. The condition showed stronger transport during NE monsoon compared to during SW monsoon.

Usually, the flow via MS is diverted to the Indian Ocean and shows strong association to the surface gradient of the sea level between part of SCS and the Andaman Sea. Wyrtki [11] has pointed out that in MS the period of strongest flow has been observed from January to April during the NE monsoon and mainly forced by the low sea level in the Andaman Sea. Thompson and Tkalich [35] reported that the volume

transport across the MS is the smallest one in the SW monsoon time. Based on our results (Table 1), transport is also greater during January (NE monsoon) than that in July (SW monsoon).

4. Conclusion

Current velocity and volume transport during January and July were studied with two-dimensional numerical models. The results obtained from this model were quite similar to SODA, HYCOM, and previous studies. SSH in MS was lower during January than during July, while SSH at part of SCS was higher during January than in July. The general circulation in MS for both January and July flows to the northwest. The reversal of wind direction changed the current velocity, but it had a little impact on the current direction. However, the general circulation in MS and SSH had a close relationship.

According to our results, MS is connected to part of SCS through SSH, current, and volume transport. SSH is always high in the south of MS compared to the north of MS. Meanwhile SSH is seasonally change in part of SCS. In MS, current and volume transport were directed to the north or the Andaman Sea both in January and July. It indicates that MS was essential in the connection between part of SCS and the Andaman Sea. The volume transport was stronger in January (NE monsoon) than July (SW monsoon) because there were NE winds, currents, and SSH gradients which were strong in part of SCS and MS.

As the difference shown in the circulation of ocean currents in the northern part of MS, we suggest that it is necessary to simulate 3D numerical models to obtain a new information on the flow and volume transport in MS especially in deep-sea topographic domains where the baroclinic influences (wind, heat, precipitation, and density) becomes important.

Acknowledgements

The authors would like to thank Muhammad Ikhwan from Graduate School of Mathematics and Applied Sciences, Universitas Syiah Kuala, Banda Aceh, Indonesia and the Ministry of Research, Technology and Higher Education which has funded this PMDSU research grant, with a contract number: 327/SP2H/LT/DRPM/IX/2016 dated on September 8, 2016. The authors would like also to thank the Faculty of Marine and Fisheries for providing research support facilities. This research is carried out in the Laboratory of Ocean Modelling, Department of Marine Sciences, Universitas Syiah Kuala, Banda Aceh, Indonesia. The author would like also to thank the anonymous reviewer who suggested significant improvements of the paper.

Table 1. Volume transport in MS along transects of 1.5°N, 3°N, and 5°N (see Fig.1) (in Sverdrup). Positive values mean the transports flow to the Andaman, and negative values mean the transports flow to the SCS.

January	July
0.21[*a], 0.22[*b], 0.21[*c], 1.14[a], 0.43[b], 1.8[c], 1.4[d], 0.0953[e]	0.14[*a], 0.14[*b], 0.13[*c], -0.19[a], -0.01[b]

**a), *b), and *c), according to our simulation along transect 1.5 °N, 3 °N, and 5 °N, respectively,*
a) According to GFDL MOM2 model [18]
b) According to GFDL MOM2 model [17]
c) According to ROMS [19]
d) According to SODA [19]
e) According to SUNTANS model [26]

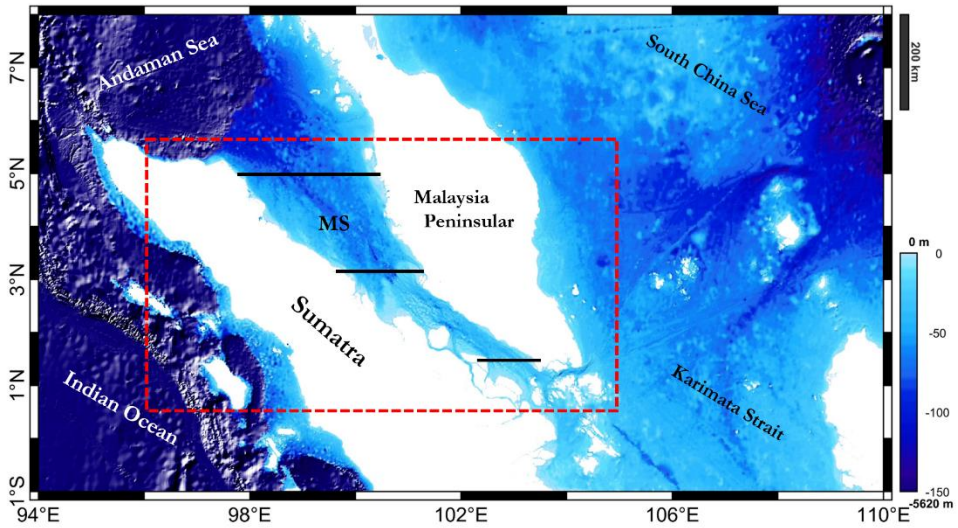

Fig. 1. The topography of the Malacca Straits and Part of South China Sea obtained from SRTM30 (in meter). The red square indicates the model domain and its edges indicate the open boundaries.

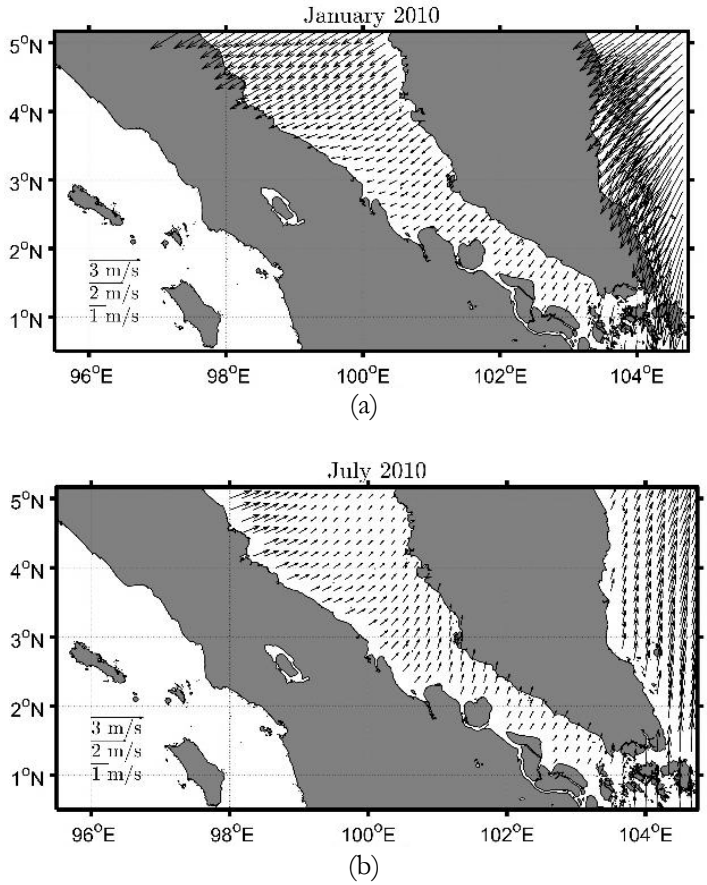

Fig. 2. Wind circulation in (a) January (NE) 2010 and (b) July (SW) 2010.

DOI:10.4186/ej.2019.23.6.129

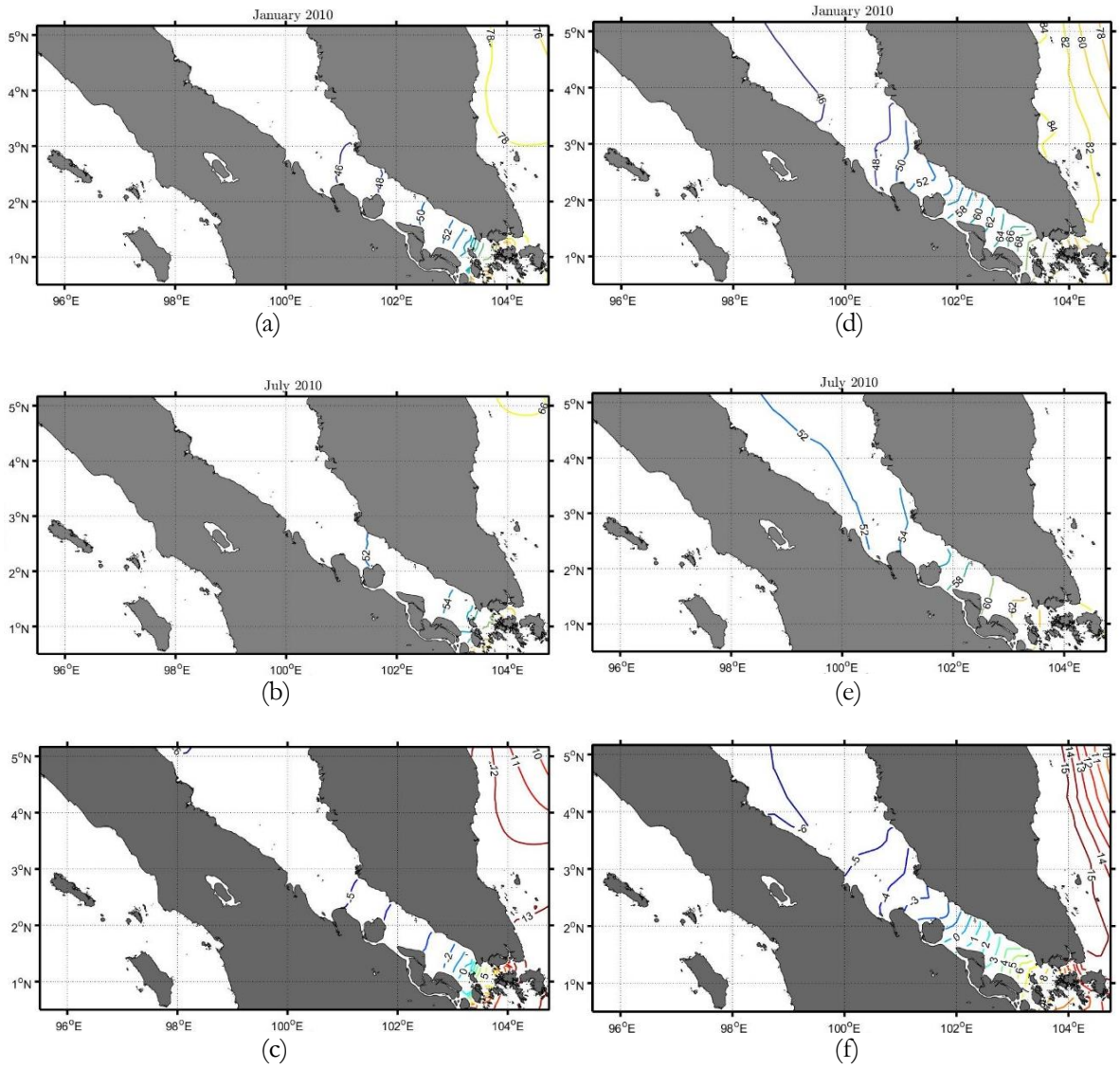

Fig. 3. SSH obtained from model simulation (a-c) and SODA (d-f). They show SSH in January (a, d) and July (b, e), and its differences (SSH in January minus SSH in July) (c, f) (x 10^{-2} m).

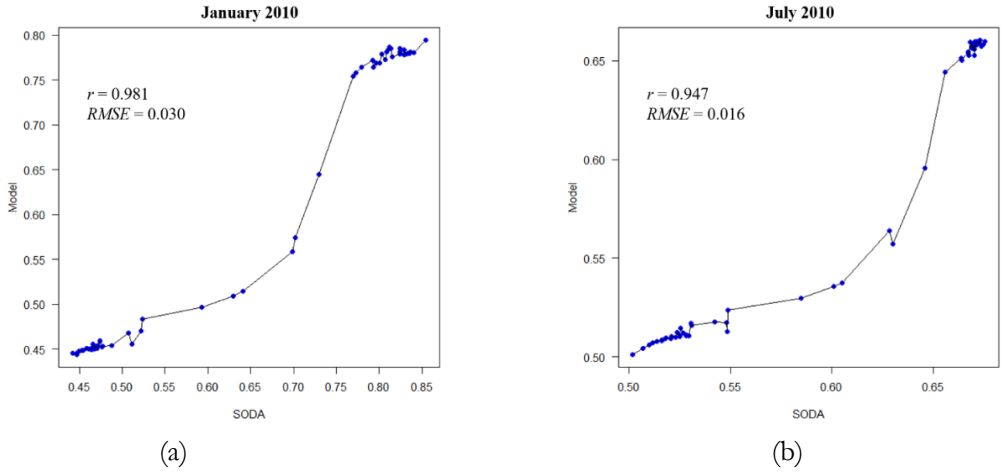

Fig. 4. The scatterplots of SSH in (a) January and (b) July obtained from model simulation vs. SODA (in unit meter).

DOI:10.4186/ej.2019.23.6.129

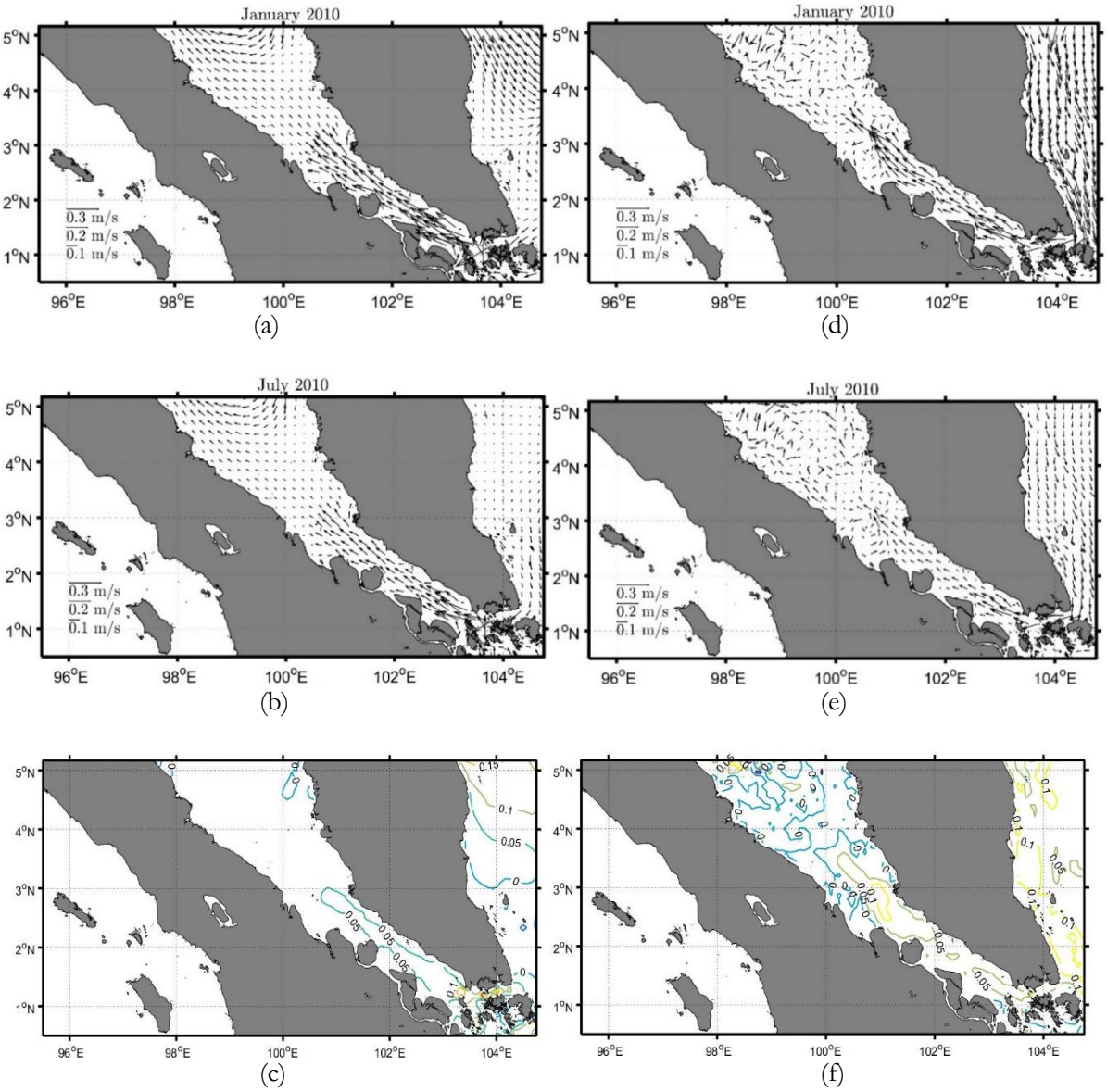

Fig. 5. Current circulation obtained from model simulation (a-c) and HYCOM (d-f). They show currents in January (a, d) and July (b, e), and their differences (currents in January minus currents in July) (c, f) (in unit m s^{-1}).

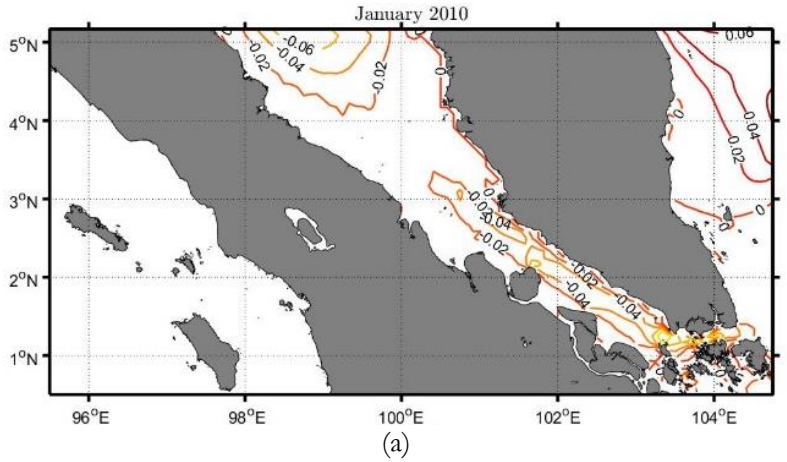

DOI:10.4186/ej.2019.23.6.129

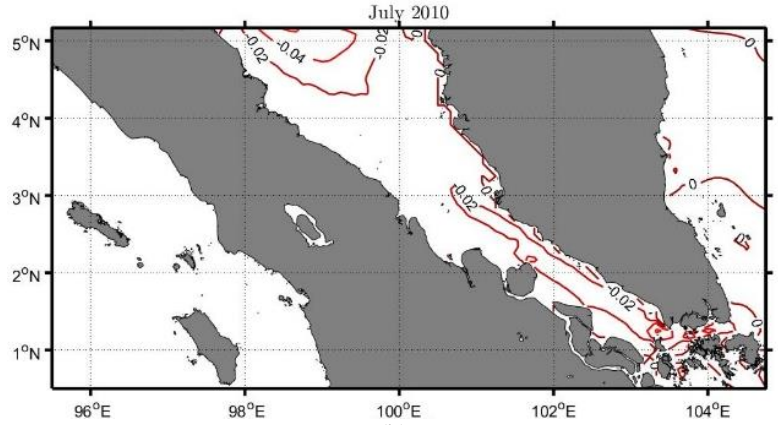

(b)

Fig. 6. U-transport in (a) January and (b) July 2010. The positive values indicate transport flow to the east while the negative values indicate transport flow to the west (in unit Sverdrup).

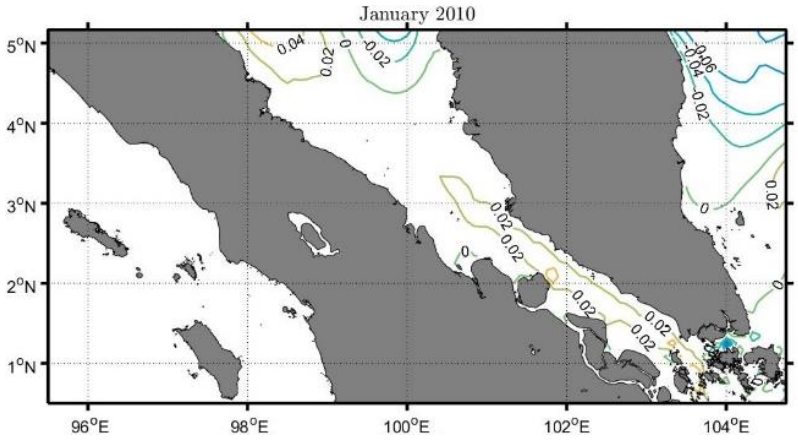

(a)

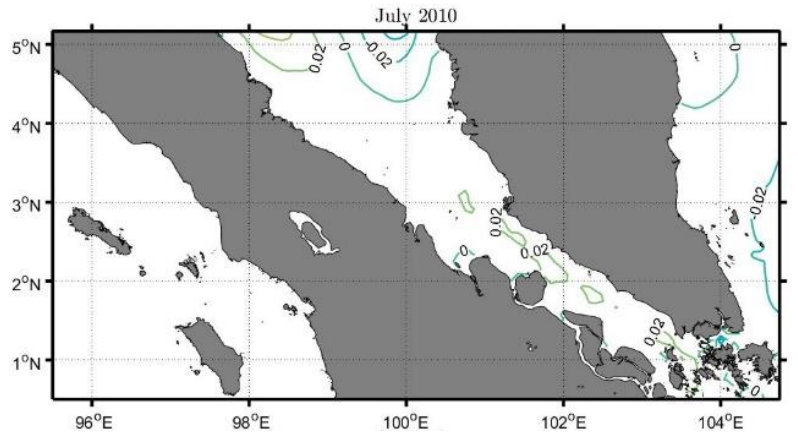

(b)

Fig. 7. V-transport in (a) January and (b) July 2010. The positive values indicate transport flow to the north while the negative values indicate transport flow to the south (in unit Sverdrup).

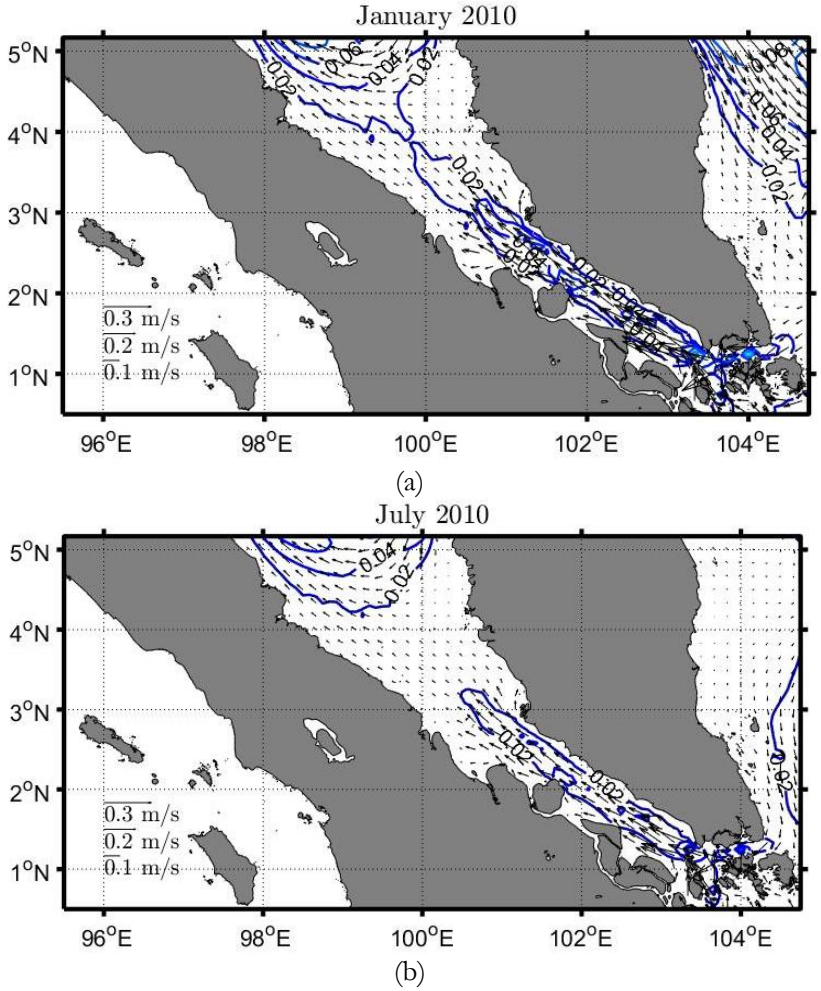

Fig. 8. The currents and magnitude of volume transport (in unit Sverdrup) in (a) January and (b) July. The currents indicate the direction of volume transport.

References

[1] H. A. Haridhi, M. Nanda, Y. Haditiar, and S. Rizal, "Application of rapid appraisals of fisheries management system (RAFMS) to identify the seasonal variation of fishing ground locations and its corresponding fish species availability at Aceh waters, Indonesia," *Ocean Coast. Manag.*, vol. 154, pp. 46-54, 2018. [Online]. Available: https://doi.org/10.1016/j.ocecoaman.2017.12.030

[2] A. S. Sakmani, W. H. Lam, R. Hashim, and H. Y. Chong, "Site selection for tidal turbine installation in the Strait of Malacca," *Renew. Sustain. Energy Rev.,* vol. 12, pp. 590-602, 2013. [Online]. Available: https://doi.org/10.1016/j.rser.2012.12.050

[3] D. Rahman, N. Sakhawat, R. Amin, and F. Ahmed, "A study on renewable energy as a sustainable alternative for ensuring energy security in Bangladesh and related socio-economic aspects," *Eng. J.*, vol. 16, no. 2, pp. 47-52, Feb. 2012. [Online]. Available: https://doi.org/10.4186/ej.2012.16.2.47

[4] A. Siripong, "Hydrodynamic and oil-spill modelling for the East Asian seas region," *AMBIO*, vol. 17, no. 3, pp. 183-185, 1998.

[5] H. Chen, P. Malanotte-Rizzoli, T. Y. Koh, and G. Song G, "The relative importance of the wind-driven and tidal circulations in Malacca Strait," *Cont. Shelf Res.,* vol. 88, pp. 92–102, 2014. [Online]. Available: https://doi.org/10.1016/j.csr.2014.07.012

[6] S. Rizal and J. Sündermann J, "On the M2-tide of the Malacca Strait: a numerical investigation," *Dtsch. Hydrogr. Zeitschrift,* vol. 46, no.1, pp. 61–80, 1994. [Online]. Available: https://doi.org/10.1007/BF02225741

[7] Y. Haditiar, S. Rizal, and F. Abdullah, "Current simulation in the Malacca Strait and part of South China Sea due to wind," in *12th International Conference on Mathematics, Statistics, and Their Applications (ICMSA)*,

Banda Aceh, Indonesia, 2016, pp. 47-50. [Online]. Available: https://doi.org/10.1109/ICMSA.2016.7954306

[8] V. Subramanian, "Hydrodynamic and transport model of the Siak Estuary," in *Coastal Environments: Focus on Asian Regions*. Dordrecht, Netherlands: Springer; 2012, ch. 11, pp. 155-172. [Online]. Available: https://doi.org/10.1007/978-90-481-3002-3

[9] S. Rizal, I. Setiawan, T. Iskandar, Y. Ilhamsyah, M. A. Wahid, and M. Musman, "Currents simulation in the Malacca straits by using three-dimensional numerical model," *Sains Malaysiana*, vol. 39, no.4, pp. 519–524, 2010.

[10] S. Rizal, P. Damm, M. A. Wahid, J. Sündermann, Y. Ilhamsyah, T. Iskandar, and Muhammad, "General circulation in the Malacca Strait and Andaman Sea: A numerical model study," *Am. J. Environ. Sci.*, vol. 8, no. 5, pp. 479–488, 2012. [Online]. Available: https://doi.org/10.3844/ajessp.2012.479.488

[11] K. Wyrtki, "Physical oceanography of the Southeast Asian waters. NAGA Report Volume 2: Scientific Results of Marine Investigations of the South China Sea and the Gulf Of Thailand 1959–1961," UC San Diego, S.I.O., La Jolla, California, 1961.

[12] S. H. X. Tay, A. Kurniawan, S. K. Ooi, and V. Babovic, "Sea level anomalies in straits of Malacca and Singapore," *Appl. Ocean Res.*, vol. 58, pp. 104–117, 2016. [Online]. Available: https://doi.org/10.1016/j.apor.2016.04.003

[13] S. Saramul, "Seasonal monsoon variations in surface currents in the Gulf of Thailand revealed by high frequency radar," *Eng. J.*, vol. 21, no. 4, pp. 25 -37, Jul. 2017. [Online]. Available: https://doi.org/10.4186/ej.2017.21.4.25

[14] S. Saramul and T. Ezer, "On the dynamics of low latitude, wide and shallow coastal system: numerical simulations of the Upper Gulf of Thailand," *Ocean Dyn.*, vol. 64, no. 4, pp. 557-571, 2014. [Online]. Available: https://doi.org/10.1007/s10236-014-0703-z

[15] G. Fang, Y. Wang, Z. Wei, Y. Fang, F. Qiao, and X. Hu, "Interocean circulation and heat and freshwater budgets of the South China Sea based on a numerical model," *Dyn. Atmos. Ocean.,* vol. 47, no. 1-3, pp. 55–72, 2009. [Online]. Available: https://doi.org/10.1016/j.dynatmoce.2008.09.003

[16] T. Qu, Y. Du, and H. Sasaki, "South China Sea throughflow : A heat and freshwater conveyor," *Geophys. Res. Lett.*, vol. 33, no. 23, pp. L23617, 2006. [Online]. Available: https://doi.org/10.1029/2006GL028350

[17] G. Fang, D. Susanto, I. Soesilo, Q. Zheng, F. Qiao, and Z. Wei, "A note on the South China Sea shallow interocean circulation," *Adv. Atmos. Sci.,* vol. 22, no. 6, pp. 946–954, 2005. [Online]. Available: https://doi.org/10.1007/BF02918693

[18] G. Fang, Z. Wei, B. H. Choi, K. Wang, Y. Fang, and W. Li, "Interbasin freshwater, heat and salt transport through the boundaries of the East and South China Sea from a variable-grid global ocean circulation model," *Sci. China, Ser. D Earth Sci.*, vol. 46, no. 2, pp. 149–161, 2003. [Online]. Available: https://doi.org/10.1360/03yd9014

[19] F. Daryabor, A. A. Samah, S. H. Ooi, and S. N. Chenoli, "An estimate of the Sunda Shelf and the Strait of Malacca transports: A numerical study," *Ocean Sci. Discuss.,* vol. 12, pp. 275–313, 2015. [Online]. Available: https://doi.org/10.5194/osd-12-275-2015

[20] W. Rukthong, P. Piumsomboon, W. Weerapakkaroon, and B. Chalermsinsuwan, "Computational fluid dynamics simulation of a crude oil transport pipeline: Effect of crude oil properties," *Eng. J.,* vol. 20, no. 3, pp. 145 -154, Aug. 2016. [Online]. Available: https://doi.org/10.4186/ej.2016.20.3.145

[21] P. Chaiwang, B. Chalermsinsuwan, and P. Piumsomboon, "Two-dimensional CFD simulation of reducing operating pressure effect on the system hydrodynamics in a downer reactor," *Eng. J.,* vol. 21, no. 2, pp. 133-149, Mar. 2017. [Online]. Available: https://doi.org/10.4186/ej.2017.21.2.133

[22] C. Kalakan, A. Sriariyawat, S. Naksuksakul, and T. Rasmeemasmuang, "Sensitivity analysis of coastal flooding to geographical factors: Numerical model study on idealized beaches," *Eng. J.,* vol. 20, no. 1, pp. 1 -15, Jan. 2016. [Online]. Available: https://doi.org/10.4186/ej.2016.20.1.1

[23] G. Han and C. L. Tang , "Interannual variations of volume transport in the western labrador sea based on TOPEX/Poseidon and WOCE data," *J. Phys. Oceanogr.,* vol. 31, 199–211, 2001. [Online]. Available: https://doi.org/10.1175/1520-0485(2001)031<0199:IVOVTI>2.0.CO;2

[24] F. Vivier and C. Provost, "Volume transport of the Malvinas Current: Can the flow be monitored by TOPEX/POSEIDON?," *J. Geophys. Res.*, vol. 104(C9), pp. 21105– 21122, 1999. [Online]. Avalaible: https://doi.org/10.1029/1999JC900056

[25] E. A. Vermeulen, B. Backeberg, J. Hermes, and S. Elipot, "Investigating the relationship between volume transport and sea surface height in a numerical ocean model," *Ocean Sci.*, vol. 15, pp. 513–526, 2019. [Online]. Available: https://doi.org/10.5194/os-15-513-2019

[26] M. Xu and V. P. Chua, "A numerical study on circulation and volume transport in Singapore coastal waters," *J. Hydro-Environment Res.,* vol. 12, pp. 70–90, 2016. [Online]. Available: https://doi.org/10.1016/j.jher.2015.11.005

[27] B. Mayer, P. E. Damm, T. Pohlmann, and S. Rizal, "What is driving the ITF? An illumination of the Indonesian throughflow with a numerical nested model system," *Dyn. Atmos. Ocean.,* vol. 50, no. 2, pp. 301–312, 2010. [Online]. Available: https://doi.org/10.1016/j.dynatmoce.2010.03.002

[28] E. Kalnay, M. Kanamitsu, R. Kistler, W. Collins, D. Deaven, L. Gandin, M. Iredell, S. Saha, G. White, J. Woollen, and Y. Zhu, "The NCEP/NCAR 40-year reanalysis project," *Bull. Am. Meteorol. Soc.*, vol. 77, pp. 437–471, 1996. [Online]. Available: https://doi.org/10.1175/1520-0477(1996)077<0437:TNYRP>2.0.CO;2

[29] J. A. Carton and B. S. Giese, "A Reanalysis of Ocean Climate Using Simple Ocean Data Assimilation (SODA)," *Mon. Weather Rev.*, vol. 136, pp. 2999-3017, 2008. [Online]. Available: https://doi.org/10.1175/2007MWR1978.1.

[30] B. S. Giese and S. Ray, "El Niño variability in simple ocean data assimilation (SODA), 1871–2008," *J. Geophys. Res.: Oceans*, vol. 116, no. C2, pp. C02024, Feb. 2011. [Online]. Available: https://doi.org/10.1029/2010JC006695

[31] S. Park and L. Xu, "Variational data assimilation for global ocean," in *Data Assimilation for Atmospheric, Oceanic and Hydrologic Applications (Vol. II)*. Heidelberg, Germany: Springer-Verlag, 2013, ch. 13, pp. 155-172. [Online]. Available: https://doi.org/10.1007/978-3-642-35088-7

[32] J. Kämpf, "Rotational effects," in *Ocean Modelling for Beginners: Using Open-Source Software*. Heidelberg, Germany: Springer-Verlag, 2009, ch. 6, sec. 8, pp. 137 - 144. [Online]. Available: https://doi.org/10.1007/978-3-642-00820-7

[33] T. Chai and R. R. Draxler, "Root mean square error (RMSE) or mean absolute error (MAE)? - Arguments against avoiding RMSE in the literature," *Geosci. Model Dev.,* vol. 7, pp. 1247–1250, 2013. [Online]. Available: https://doi.org/10.5194/gmd-7-1247-2014

[34] Y. Jin, C. B. Schaaf, F. Gao, X. Li, A. H. Strahle, W. Lutch, and S. Liang, "Consistency of MODIS surface bidirectional reflectance distribution function and albedo retrievals: 2. Validation," *J. Geophys. Res.*, vol. 108, pp. 4159, 2003. [Online]. Available: https://doi.org/10.1029/2002JD002804

[35] B. Thompson and P. Tkalich, "Mixed layer thermodynamics of the Southern South China Sea," *Clim. Dyn.*, vol. 43, no. 7 -8, pp. 2061–2075, 2014. [Online]. Available: https://doi.org/10.1007/s00382-013-2030-3

[36] D. Xu and P. Malanotte-Rizzoli, "The seasonal variation of the upper South layers of the China Sea (SCS) Circulation and Indonesian the through flow (ITF): An ocean study model," *Dyn. Atmos. Ocean.*, vol. 63, pp. 103-130, 2013. [Online]. Available: https://doi.org/10.1016/j.dynatmoce.2013.05.002